2020 IEEE PELS Workshop on Emerging Technologies: Wireless Power Transfer (WoW)
November 15 - 19, 2020, Seoul, Korea

A Linear Extendable Phase-shift Controlled Multi-coil Transmitter Architecture for Wireless Power Transfer with 3D Magnetic Field Shaping

1st Ning Kang
University of Michigan-Shanghai Jiao Tong University Joint Institute, Shanghai Jiao Tong University,
Shanghai, China
corningkdc@sjtu.edu.cn

2nd Chengbin Ma
University of Michigan-Shanghai Jiao Tong University Joint Institute, Shanghai Jiao Tong University,
Shanghai, China
chbma@sjtu.edu.cn

3rd Ming Liu
Department of Electrical Engineering, Princeton University,
Princeton, US
ml45@princeton.edu

***Abstract*—Wireless power transmission (WPT) systems operating at MHz have advantages of small size and a high tolerance for coils misalignment. There is an urgent need for existing MHz WPT systems to improve coupling coils efficiency and positional freedom of the receiver simultaneously. There exist some ways for improving coils efficiency and positional freedom of the receiver, such as introducing repeater coils and employing special coils structures. However, lack of magnetic field strength can limit the freedom of the receiver, and the excessive coupling may cause inefficiency in coils. This paper proposes a phase-shift controlled multi-coil transmitter architecture. The architecture is linear extendable and it enables the 3D magnetic field shaping, which helps to improve the coupling coils efficiency and the spatial freedom of the receiver. The design of the compensation capacitors of the transmitting coils is discussed to achieve the optimal operation for the high-frequency power amplifier (PA) when considering the effect of the cross-coupling among transmitting coils. The mathematic model for the 3D magnetic field shaping is derived to prove the concept of the approach. The calculation results show the capability of 3D magnetic field shaping when using a two-coil transmitter as an example. The experimental results match well with the theoretical analysis and the simulation results. Three WPT systems are studied in the paper. Compared with the single transmitter system (STS) and the two-coil transmitter system (TTS) without phase-shift control (PSC), the TTS with PSC can maintain higher system efficiency in three degrees of freedom (vertical movement, horizontal movement, flip with fixed axis). In particular, only the TTS with PSC can work when the receiving coil is perpendicular to the transmitting coils. Therefore, due to the ability to shape the 3D magnetic field, the linear extendable multi-coil transmitter architecture with PSC has advantages in terms of the receiver freedom and the coupling coils efficiency.**

***Index Terms*—wireless power transfer, MHz, phase-shift control, multi-coil transmitter architecture, two-coil transmitter.**

I. Introduction

WPT technologies have been widely applied to the charging of wearable devices, mobile phones, and even electric cars. Most current WPT systems operate in the kilohertz (kHz) band. Through improvements in compensation topology, coil design, and control, numerous novel efforts have been made to improve the performance of KHz systems [1]–[3]. On the other hand, higher operating frequencies, such as several megahertz (MHz), can further improve the spatial freedom of the WPT system, which is longer transmission distances and better tolerance to coil misalignment [4]. Higher operating frequencies also help achieve a more compact and lighter WPT system. However, since the magnetic field distribution of resonant coils is usually unchangeable, it is hard to improve the spatial freedom without reducing the high efficiency of coils. Thus, there is still an urgent need for existing MHz WPT systems to improve coupling coils efficiency and positional freedom of the receiver simultaneously. For the above reasons, magnetic field shaping technology has been attracting growing interest [5], [6].

Magnetic field shaping technologies allow control of the magnetic flux at a particular location and reduce excessive coupling coefficient, thereby improving positional freedom and coils efficiency simultaneously. Note that both weak coupling and excessive coupling are detrimental to WPT systems. When the coupling coefficient is small, the transmission freedom of the WPT system will be limited. Conversely, an excessive coil coupling coefficient is also detrimental to the efficiency and stability of the WPT system. The reason is that an excessive coupling coefficient will cause the power amplifier (PA) to see a large impedance, which is not conducive to the operation of the PA. Besides, quality factors should be large enough for the coupling coils to work stably under the strong coupling. Generally, magnetic field shaping technologies are divided into two categories, namely passive methods and active methods. Passive methods exploit magnetic cores to provide low reluctance paths for the magnetic flux, but such an approach can significantly increase the size and weight of the transmitter and receiver [7]. Active methods achieve magnetic field shaping by changing the distribution of currents in the transmitters [8]. To improve the WPT systems by magnetic field shaping, some state-of-art methods have been proposed [9], [10]. However, in order to avoid cross-coupling between the transmitting coils, these coils are designed to be bulky 3D structures, which obviously limits the application scenarios. Besides, these systems operate at lower frequencies, making

978-1-7281-3746-9/20/$31.00 ©2020 IEEE

the power amplifier and rectifier larger and heavier.

This paper presents a 2D multi-coil transmitter architecture with phase-shift control. The linearly extendable architecture can implement 3D magnetic field shaping, thus to help MHz systems to improve the efficiency of coils and the spatial freedom of the receiver. The paper is organized as follows. Section II gives the multi-coil transmitter architecture. And the circuit structure of a two-coil transmitter system is proposed and analyzed as an example implementation of multi-coil transmitter architecture with PSC. Applying Biot-Savart law, section III develops the magnetic field generated by the two-coil transmitter. Then section IV validates the analytical results by experiments using the three example 6.78-MHz WPT systems, namely STS, TTS without PSC, and TTS with PSC. All the three example WPT systems are studied from DC input end to DC output end in three degrees of receiver freedom. Finally, section V draws the conclusions.

II. Transmitter Architecture

Fig. 1 shows the concept of the linear extendable multi-coil transmitter architecture. The transmitter consists of multiple coils and each coil is driven by a power amplifier with PSC. As shown in the figure, the transmitter can extended from two coils (2x1) to twenty five coils (5x5). This feature enables the proposed transmitter architecture work with different wireless power transfer applications. By modulating the phase-shift among all the coils, different 3D magnetic field can be shaped. As an example of the proposed extendable multi-coil transmitter architecture with PSC, Fig. 2 shows an implementation of an MHz WPT system with a phase-shift controlled two-coil transmitter. The transmitter side comprises two Class D power amplifiers operating at 6.78 MHz and two transmitting coils. And the receiver side comprises a receiving coil and a full-wave rectifier. By controlling the phase difference between the two drive signals of PAs, the two transmitting coils will obtain different-phase currents.

The input impedance of the Class E full-wave rectifier, Z_{rec}, is as follows:

$$Z_{\text{rec}} = R_{\text{rec}} + jX_{\text{rec}} \tag{1}$$

where R_{rec} is the resistance and X_{rec} is the reactance. To compensate for the reactance of the rectifier, the optimal compensation capacitance of the receiving coil needs to satisfy the following relationship

$$C_{\text{rx}} = \frac{1}{\omega\left(\omega L_{\text{rx}} + X_{\text{rec}}\right)} \tag{2}$$

where L_{rx} is the inductances of the receiving coil, and ω is the resonance frequency of the WPT system, i.e., 6.78 MHz here.

For coupling coils, the power loss occurs on the parasitic resistances, i.e., r_{tx} and r_{rx}. For simplicity, the transmitting and receiving coils are identical in TTS. Thus, the following conditions are met: $r_{tx} = r_{rx} = r$ and $L_{tx} = L_{rx} = L$. For a fair comparison, the inductance and resistance of the transmitting coil in STS are $2r$ and $2L$, respectively. Applying

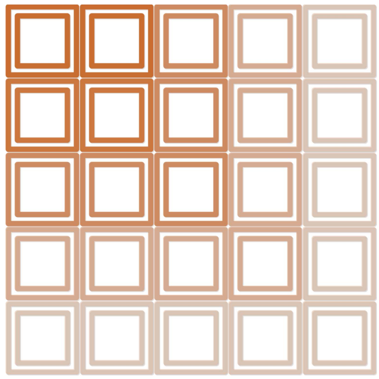

Fig. 1. Concept of the linear extendable multi-coil transmitter architecture.

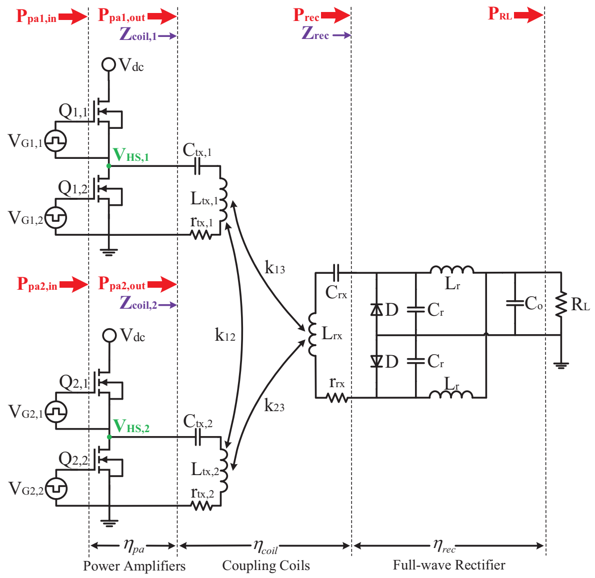

Fig. 2. An example implementation of MHz WPT system with a phase-shift controlled two-coil transmitter.

the derivation of [11], the input impedance and efficiency of coupling coils in traditional STS can be expressed as follows

$$Z_{\text{in}} = 2r + \frac{2\omega^2 k^2 L^2}{r + R_{\text{rec}}} \tag{3}$$

$$\eta_{\text{coils}} = \frac{R_{\text{rec}}}{R_{\text{rec}} + r}\left(1 + \frac{r}{\frac{\omega^2 k^2 L^2}{R_{\text{rec}}+r}}\right) \tag{4}$$

Z_{in} is purely resistive in the case of satisfying the optimum compensation capacitance.

Similarly, input impedance and efficiency of each coil in TTS are shown as

$$Z_{\text{ins}} = r + \frac{\omega^2 k^2 L^2}{r + R_{\text{rec}}} + \frac{\omega^2 k_{12}^2 L^2}{r + R_{\text{pa}}} \tag{5}$$

$$\eta_{\text{coils}} = \frac{R_{\text{rec}}}{R_{\text{rec}} + r}\left(1 + \frac{r}{\frac{\omega^2 k^2 L^2}{R_{\text{rec}}+r} + \frac{\omega^2 k_{12}^2 L^2}{R_{\text{pa}}+r}}\right) \tag{6}$$

where R_{pa} represents the input impedance seen from the transmitting coil end of another PA. And k_{12} is the cross-coupling coefficient between the two coils. The left side of the following inequality is obtained by comparing the different parts of (4) and (6),

$$\frac{\omega^2 k_c^2 L^2}{R_{\text{pa}} + r} > 0 \tag{7}$$

The above inequality implies that the coil efficiency of TTS is greater than the coil efficiency of STS, which can be expressed as

$$\eta_{\text{coils}} > \eta_{\text{coil}} \tag{8}$$

The conclusion can also be drawn from impedance analysis. For one transmitting coil in TTS, the cross-coupling of the other transmitting coil increases the reflected impedance seen by the transmitting coil. When the transmitting coil has constant parasitic resistance, a larger input impedance means higher efficiency.

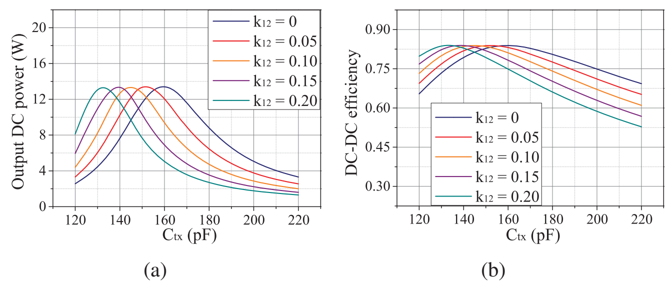

Fig. 3. The simulation results of TTS using Advanced Design System (ADS). (a) The system efficiency of TTS. (b) The output performance of TTS.

The two resonance capacitors, $C_{tx,1}$ and $C_{tx,2}$, play an important role in PSC. These capacitors must be carefully designed so as to the two PAs both see the inductive load. Fig. 3 shows the simulation results of output power and the efficiency of TTS using ADS. Here, k_{13} and k_{23} are equal to 0.1 and remain unchanged in the simulation. Besides, $C_{tx,1}$ and $C_{tx,2}$ are the same. The figure shows that C_{tx} significantly affects output power and efficiency of TTS under different cross-coupling coefficients. For Fig. 3(a), with the increase of the cross-coupling coefficient, the peak values of output power gradually move towards the direction where C_{tx} decrease. This observation is consistent with the results in Fig. 3(b). In practice, the capacitance of $C_{tx,1}$ and $C_{tx,2}$ also needs to be adjusted according to the other parts of the circuit.

III. 3D Magnetic Field Shaping

In this section, the magnetic field (B-field) generated by the two-coil transmitter is studied as a general B-field analysis of the multi-coil transmitter architecture with phase-shift control. Applying Biot-Savart's law, the magnetic induction produced by a coil with the current is defined as

$$B = \frac{\mu_0}{4\pi} \oint_C \frac{I d\boldsymbol{l} \times \boldsymbol{r}}{|r|^3} \tag{9}$$

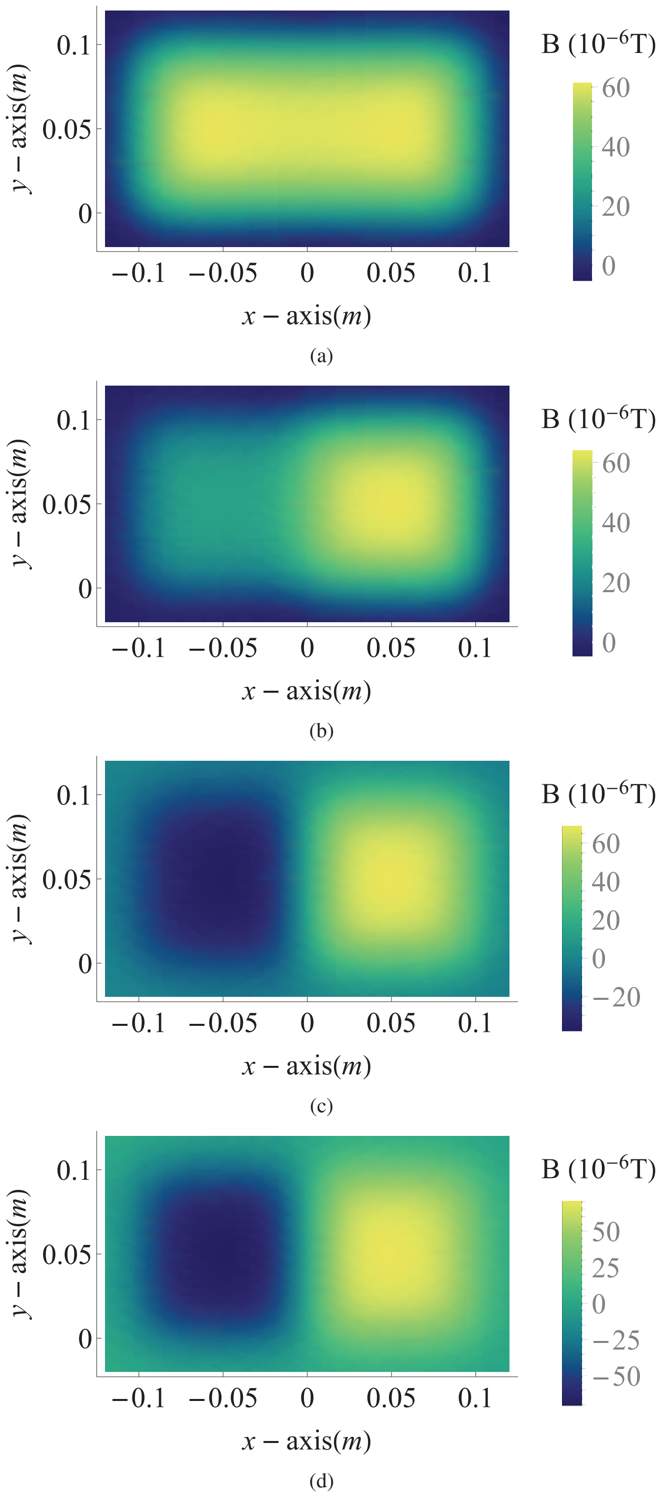

Fig. 4. Calculation results of z-direction B-field generated by two flat transmitting coils with different θ (d=3.60cm). (a) The z-direction B-field of θ=0. (b) The z-direction B-field of $\theta = 60°$. (c) The z-direction B-field of $\theta = 120°$. (d) The z-direction B-field of $\theta = 180°$.

where $\boldsymbol{dl}$ is a vector along the path C whose magnitude is the length of the differential element of the coil. And $\boldsymbol{r}$ is a displacement vector from the coil element ($\boldsymbol{dl}$) to the point at which the field is being computed. The magnetic constant is expressed by μ_0. Then, the magnetic field generated by a rectangular coil flowing through a sinusoidal current at a certain point can be found that

$$B_0 = \oint_C \frac{\mu_0 n I_0 \cos(\omega t)}{4\pi r^2} \boldsymbol{dl} \times \boldsymbol{r} \tag{10}$$

Note that n represents the number of coil turns, I_0 is the same current amplitude in two coils, and θ is the phase difference of the currents in the two coils. The total magnetic induction generated by two coils is as follows:

$$B_t = B_1 + B_2 \tag{11}$$

Since only rectangular coils are used in this paper, the loop integral in (10) can be decomposed into four integral for lines. Then, the side length of the same rectangular coils is defined as $2l$. Finally, the components of magnetic induction in directions x, y, and z can be derived as

$$B_{tx} = \frac{\mu_0 n I_0 z}{4\pi}\{\cos(\omega t)(a-b)+\cos(\omega t+\theta)(-c+d)\} \tag{12}$$

$$B_{ty} = \frac{\mu_0 n I_0 z}{4\pi}\{\cos(\omega t)(-e+f)+\cos(\omega t+\theta)(-g+h)\} \tag{13}$$

$$\begin{aligned} B_{tz} = \frac{\mu_0 n I_0}{4\pi}\{&\cos(\omega t)(ye - xa - (-2l+y)f + (2l+x)b) \\ &+ \cos(\omega t+\theta)(yg + xc - (-2l+y)h - (-2l+x)d)\} \end{aligned} \tag{14}$$

Note that the eight parameters a, b, c, d, e, f, g, and h are determined by the spatial position of the observation point, which can be represented as follows

$$a = \frac{-\frac{y}{\sqrt{x^2+y^2+z^2}} + \frac{-2l+y}{\sqrt{x^2+(-2l+y)^2+z^2}}}{x^2+z^2} \tag{15}$$

$$b = \frac{-\frac{y}{\sqrt{(2l+x)^2+y^2+z^2}} + \frac{-2l+y}{\sqrt{(2l+x)^2+(-2l+y)^2+z^2}}}{(2l+x)^2+z^2} \tag{16}$$

$$c = \frac{-\frac{y}{\sqrt{x^2+y^2+z^2}} + \frac{-2l+y}{\sqrt{x^2+(-2l+y)^2+z^2}}}{x^2+z^2} \tag{17}$$

$$d = \frac{-\frac{y}{\sqrt{(-2l+x)^2+y^2+z^2}} + \frac{-2l+y}{\sqrt{(-2l+x)^2+(-2l+y)^2+z^2}}}{(-2l+x)^2+z^2} \tag{18}$$

$$e = \frac{\frac{x}{\sqrt{x^2+y^2+z^2}} + \frac{-2l-x}{\sqrt{(2l+x)^2+y^2+z^2}}}{y^2+z^2} \tag{19}$$

$$f = \frac{\frac{x}{\sqrt{x^2+(-2l+y)^2+z^2}} + \frac{-2l-x}{\sqrt{(2l+x)^2+(-2l+y)^2+z^2}}}{(-2l+y)^2+z^2} \tag{20}$$

$$g = \frac{-\frac{x}{\sqrt{x^2+y^2+z^2}} + \frac{-2l+x}{\sqrt{(-2l+x)^2+y^2+z^2}}}{y^2+z^2} \tag{21}$$

$$h = \frac{-\frac{x}{\sqrt{x^2+(-2l+y)^2+z^2}} + \frac{-2l+x}{\sqrt{(-2l+x)^2+(-2l+y)^2+z^2}}}{(-2l+y)^2+z^2} \tag{22}$$

In the calculation, two transmitting coils are placed in the xy plane with a zero z coordinate.

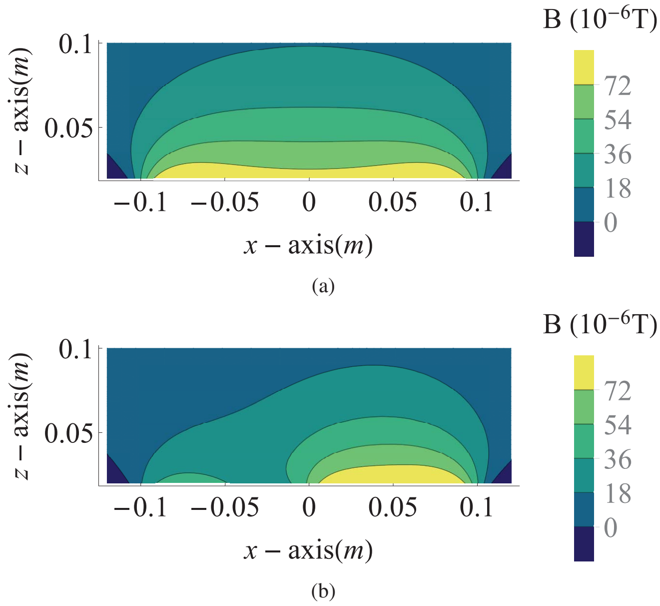

Fig. 5. Calculation results of z-direction B-field generated by two flat transmitting coils with different θ (y=5.00cm). (a) The z-direction B-field of θ=0. (b) The z-direction B-field of $\theta = 60°$.

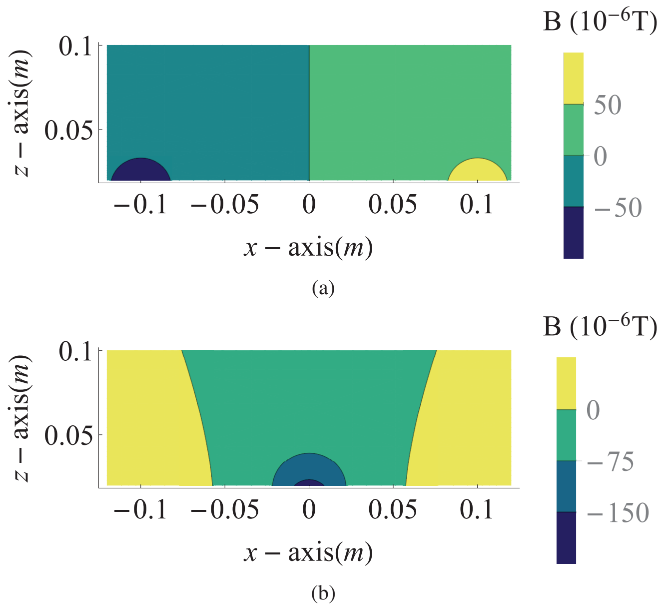

Fig. 6. Calculation results of x-direction B-field generated by two flat transmitting coils with different θ (y=5.00cm). (a) The x-direction B-field of θ=0. (b) The x-direction B-field of $\theta = 180°$.

According to the above equation, we can compare the difference of the magnetic fields generated by the two transmitting coils in TTS under various phase differences. Fig. 4 shows the calculation results of magnetic induction distribution (B-field) at the same height level when θ changes from 0 degrees to 360 degrees. Note that d means the height of the horizontal plane from the transmitting coils. The peak value of the magnetic field is proportional to the peak value of the induced voltage on the receiving coil, which is related to the received power. For a fair comparison, each picture is fixed at the moments in which the B-field has the maximum strength [refer to Fig. 4, Fig. 5, and Fig. 6]. The figure especially demonstrates that the peak of the magnetic field moves laterally as the phase difference increases. This possibility can be fully utilized to adapt the horizontal misalignment of the MHz WPT systems, as discussed in Section IV.

Similarly, the calculation results of B-field in Fig. 5 serves as a general example to analyze the ability of phase difference to control the B-field in the z-direction at different heights. The figure illustrates the ability of TTS with PSC to adapt to the different transmission distances. Again, as shown in Fig. 6, the B-field along the x-direction is different when the phase differences are 0 degrees and 180 degrees. Unlike the case where the θ is 0 degrees, the transverse B-field on the middle vertical line (x = 0) is not 0 when θ is 180 degrees. The figure demonstrates that TTS with PSC has the ability to charge the receiving coil with flip angles (even perpendicular to the transmitting coils), which is hard to realize in STS. Here, the observation surface is the same in Fig. 5 and Fig. 6, but they show magnetic fields in different directions.

Note that the strength of the B-field in three degrees of freedom can be changed by changing the phase difference of the current in the transmitting coils, thus increasing the energy obtained by the receiving coil or successfully avoiding the over-coupling at a short distance. Besides, changing the phase difference can also adjust the impedance seen by each power amplifier, allowing the power amplifier to operate in a more ideal state.

IV. Experimental Results

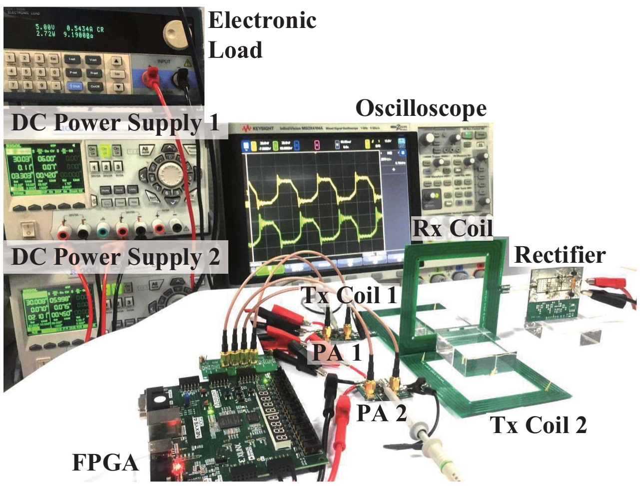

Fig. 7. A prototype two-coil transmitter WPT system with phase-shift control. In this figure, the receiving coil is perpendicular to the transmitting coils.

Fig. 7 shows an example implementation of MHz WPT system with a phase-shift controlled two-coil transmitter. The system can verify the proposed multi-coil transmitter architecture with phase-shift control at the system level. The two transmitting coils are placed on a horizontal surface and fixed in position. A DC load is emulated using an electronic load. In order to achieve better PSC performance, the circuit model and parameters of two PAs are the same as given in Fig. 2. The MHz frequency switches are GaN transistors (GS61004B) operating in 6.78MHz. In the coupling coils, the capacitances C_{tx} and C_{rx} are 172 pF and 192 pF, respectively. These design parameters are chosen based on specifications of the switching devices and the design guidance in Section II.

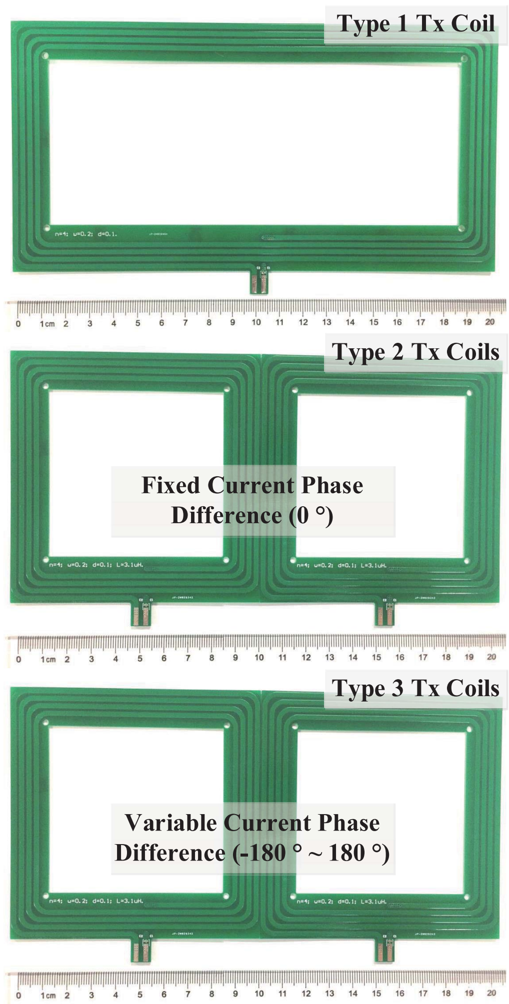

Fig. 8. Three types of transmitting coil(s).

Three experimental 6.78-MHz WPT systems, namely STS, TTS without PSC, and TTS without PSC, are built up employing three types of transmitting coil(s). As shown in Fig. 8, the only difference between the three WPT systems is the transmitting coils. Note that circuit parameters in STS are also optimized based on its transmitting coil. The coverage area of the three types of transmitting coils is the same (20cm∗10cm). Besides, the three types of coils also have the same number of turns, line width, line spacing, and line thickness. Major parameters of transmitting coils are listed in Table I. Note that the large coil has a lower quality factor than smaller coils since parasitic resistance grows faster than inductance as the coil size increases. Based on the three WPT systems, the proposed magnetic field shaping methods can be experimentally verified and compared.

TABLE I
MAJOR PARAMETERS OF TRANSMITTING COILS.

Types of tx coils	Type 1	Type 2	Type 3
Inductance (μH)	6.27	3.45	3.45
Parasitic resistance (Ω)	0.78	0.31	0.31
Number of turns	4	4	4

In case 1, all coils are fixed and the receiving coil is horizontally placed above the transmitting coils. Here, the current phase difference between the two transmitting coils is adjustable. Fig. 10(a) and Fig. 10(b) show the experimental results of the output power and the system efficiency under different θ of PAs. It shows that the system output power and the efficiency decrease first and then increase as the phase difference increases. As shown in Fig. 4, when the phase difference increases from 0 degrees to 180 degrees, the positive and negative magnetic flux passing through the coil placed in the middle will cancel each other. Note that TTS is well designed since the maximum efficiency of the system is over 80% when the phase difference is 0 degrees. Key experimental waveforms of the Class D PAs with PSC are shown in Fig. 11, in which V_{HS} is the voltage of the below transistor [see Fig. 2].

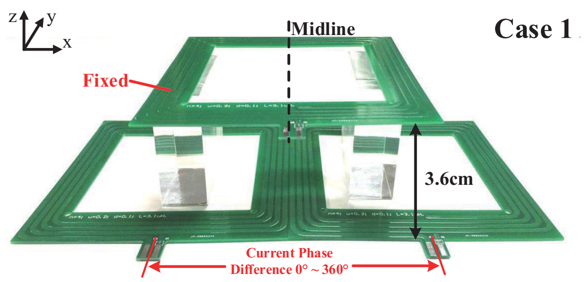

Fig. 9. Charging case 1 for TTS: scanning the phase difference of coils when receiving coil is fixed.

In case 2, the horizontal receiving coil moves vertically on the midline [see Fig. 12]. Fig. 13 shows two systems, TTS without PSC and TTS with PSC, perform the same in terms of the output power and system efficiency. As shown in Fig. 4(a), a uniform magnetic field is formed near the midline when the θ is 0 degrees. Since the receiving coil is in a symmetrical position in case 2, the optimized current phase differences for TTS is 0 degrees. Note that the output power and efficiency of the STS are much lower than those of the other two TTSs.

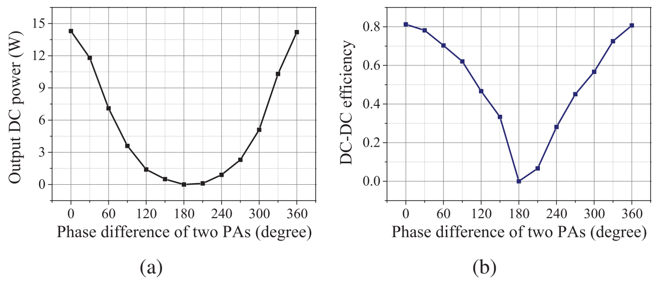

Fig. 10. Experimental results for case 1 with the phase difference changing from 0 degrees to 360 degrees. (a) The output performance of TTS. (b) The system efficiency of the TTS.

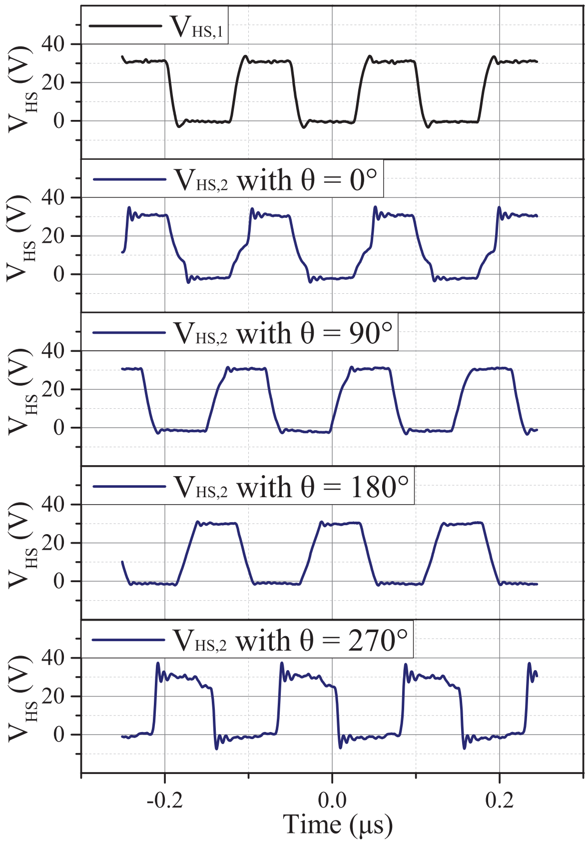

Fig. 11. Key experimental waveforms of the Class D PAs with PSC.

The reason is that the PA of STS works under a large load and the efficiency of the coils is low [refer to Section II]. The optimized phase differences for TTS with PSC in case 2 are listed in Table II.

TABLE II
THE OPTIMIZED θ FOR TTS WITH PSC IN CASE 2.

Vertically distance (cm)	1.8	2.7	3.6	4.5	5.4
Optimized θ (Degree)	0	0	0	0	0

In case 3, although the receiving coil also moves vertically, the PSC plays an important role since the coil deviates from

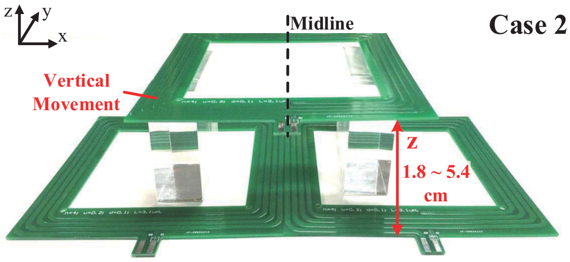

Fig. 12. Charging case 2 for three WPT systems: the horizontal receiving coil moves vertically on the midline.

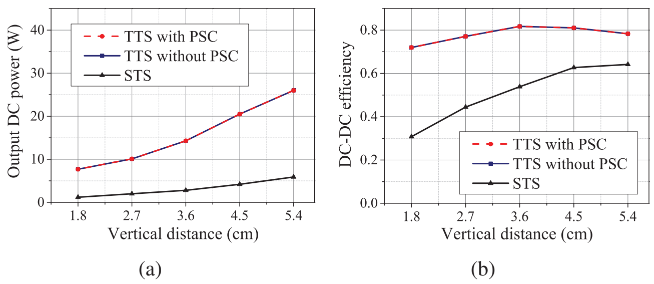

Fig. 13. Experimental results for case 2 with the vertical distance changing from 1.8cm to 5.4 cm. (a) The output performance of STS, TTS without PSC, and TTS with PSC. (b) The system efficiency of STS, TTS without PSC, and TTS with PSC.

the midline. In Fig. 15(a) and Fig. 15(b), TTS with PSC shows a clear system efficiency advantage at the same output power level. Magnetic fields of different heights can be controlled by θ, and the unnecessary fluxes are reduced so as to improve coils efficiency [see Fig. 5]. Table III lists the optimized phase differences for TTS with PSC in case 3.

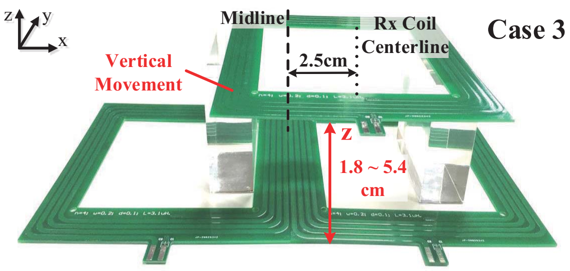

Fig. 14. Charging case 3 for three WPT systems: the horizontal receiving coil moves vertically at a distance of 2.5cm from the midline.

TABLE III
THE OPTIMIZED θ FOR TTS WITH PSC IN CASE 3.

Vertically distance (cm)	1.8	2.7	3.6	4.5	5.4
Optimized θ (Degree)	70	50	35	25	10

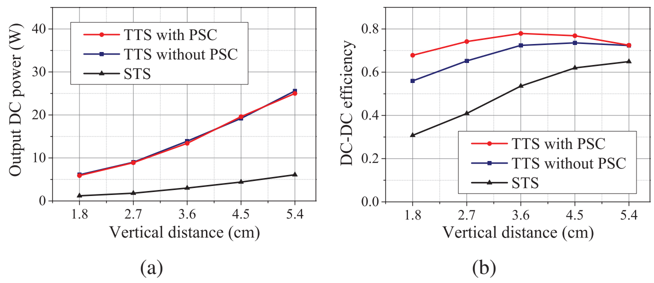

Fig. 15. Experimental results for case 3 with the vertical distance changing from 1.8cm to 5.4 cm. (a) The output performance of STS, TTS without PSC, and TTS with PSC. (b) The system efficiency of STS, TTS without PSC, and TTS with PSC.

In case 4, PSC still benefits WPT systems when the receiving coil moves horizontally at a 3.6cm height [refer to Fig. 16]. Fig. 17(a) and Fig. 17(b) show that TTS with PSC also has the advantage of system efficiency compared with the other two systems. As shown in Fig. 4, θ can control the position of B-field peaks in the horizontal plane. The optimized phase differences for TTS with PSC in case 4 are listed in Table IV.

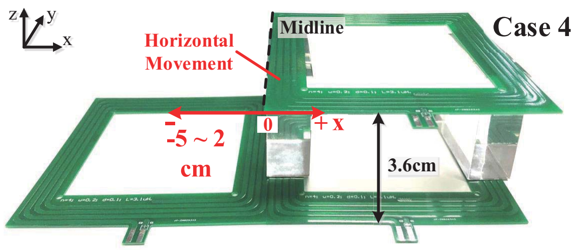

Fig. 16. Charging case 4 for three WPT systems: the horizontal receiving coil moves horizontally at a 3.6cm height.

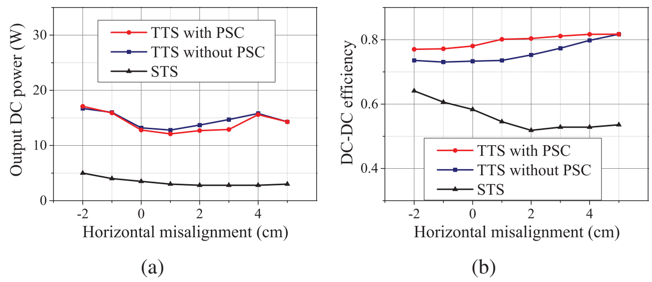

Fig. 17. Experimental results for case 4 with the horizontal distance changing from -2cm to 5 cm. (a) The output performance of STS, TTS without PSC, and TTS with PSC. (b) The system efficiency of STS, TTS without PSC, and TTS with PSC.

In case 5, the receiving coil flips with a fixed axis. Particularly, only TTS with PSC can work when the receiving coil is perpendicular to the transmitting coils [see Fig. 19(a) and Fig. 19(b)], which is in line with the analysis of Fig. 6 in Section III. In the experiments, both STS and TTS without PSC show PA overcurrent and no output power. However, at 60-degree flip angle, the advantages of TTS are not as obvious

TABLE IV
THE OPTIMIZED θ FOR TTS WITH PSC IN CASE 4.

Misalignment (cm)	-2	-1	0	1	2	3	4	5
Optimized θ (Degree)	30	40	45	55	50	40	15	0

as that in the case 4 and case 5. It is because that STS is more adapted to the coupling coefficient at the above flip angle. Table V lists the optimized phase differences for TTS with PSC in case 5.

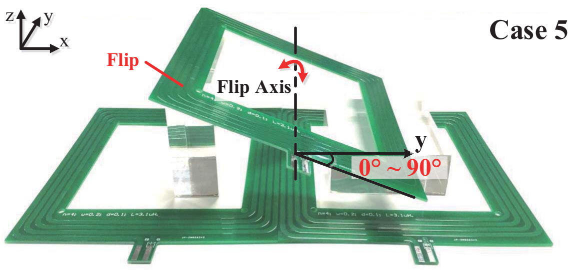

Fig. 18. Charging case 5 for three WPT systems: the receiving coil flips with a fixed axis.

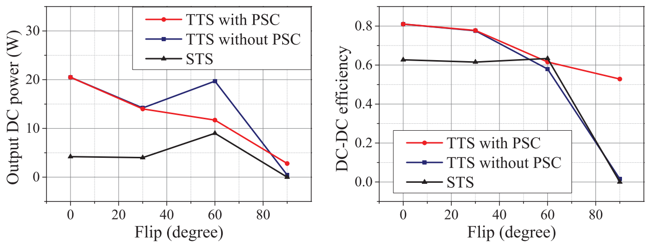

(a) (b)

Fig. 19. Experimental results for case 5 with the flip angles changing from 0 degrees to 90 degrees. (a) The output performance of STS, TTS without PSC, and TTS with PSC. (b) The system efficiency of STS, TTS without PSC, and TTS with PSC.

TABLE V
THE OPTIMIZED θ FOR TTS WITH PSC IN CASE 5.

Flip angles (Degree)	0	30	60	90
Optimized θ (Degree)	360 (0)	350	300	190

V. CONCLUSIONS

This paper proposes a phase-shift controlled multi-coil transmitter architecture, which is linear extendable. And the architecture enables the 3D magnetic field shaping so as to improve the coupling coils efficiency and the spatial freedom of the receiver. In order to achieve the optimal operation for the high-frequency power amplifiers, the compensation capacitors of the transmitting coils are studied when considering the effect of the cross-coupling among transmitting coils. Then, we developed the theory of 3D magnetic field shaping for 2D coils architecture and proposed a method to improve the receiver freedom and coils efficiency. All the three example WPT systems, namely STS, TTS without PSC, and TTS with PSC, are studied from DC input end to DC output end in three degrees of the receiver freedom. Compared with the STS and the TTS without PSC, the TTS with PSC can ensure higher system efficiency in the three degrees of freedom. In particular, only the TTS with PSC can work when the receiving coil is perpendicular to the transmitting coils. Experimental results are reasonably explained by the theoretical calculations and the simulation analysis. Therefore, given the ability to shape the 3D magnetic field mentioned above, the proposed linear extendable multi-coil transmitter architecture with phase-shift control has advantages in both the receiver freedom and the coupling coils efficiency.

REFERENCES

[1] R. Hua and A. P. Hu, "Modeling and analysis of inductive power transfer system with passive matrix power repeater," *IEEE Transactions on Industrial Electronics*, vol. 66, no. 6, pp. 4406–4413, 2018.
[2] T. Kan, T.-D. Nguyen, J. C. White, R. K. Malhan, and C. C. Mi, "A new integration method for an electric vehicle wireless charging system using lcc compensation topology: Analysis and design," *IEEE Transactions on power electronics*, vol. 32, no. 2, pp. 1638–1650, 2016.
[3] C. C. Mi, G. Buja, S. Y. Choi, and C. T. Rim, "Modern advances in wireless power transfer systems for roadway powered electric vehicles," *IEEE Transactions on Industrial Electronics*, vol. 63, no. 10, pp. 6533–6545, 2016.
[4] S. Y. R. Hui, W. Zhong, and C. K. Lee, "A critical review of recent progress in mid-range wireless power transfer," *IEEE Transactions on Power Electronics*, vol. 29, no. 9, pp. 4500–4511, 2013.
[5] B.-H. Choi, B.-C. Park, and J.-H. Lee, "Near-field beamforming loop array for selective wireless power transfer," *IEEE Microwave and Wireless Components Letters*, vol. 25, no. 11, pp. 748–750, 2015.
[6] Y. H. Sohn, B. H. Choi, E. S. Lee, and C. T. Rim, "Comparisons of magnetic field shaping methods for ubiquitous wireless power transfer," in *2015 IEEE PELS Workshop on Emerging Technologies: Wireless Power (2015 WoW)*. IEEE, 2015, pp. 1–6.
[7] S. Santalunai, C. Thongsopa, and T. Thosdeekoraphat, "An increasing the power transmission efficiency of flat spiral coils by using ferrite materials for wireless power transfer applications," in *2014 11th International Conference on Electrical Engineering/Electronics, Computer, Telecommunications and Information Technology (ECTI-CON)*. IEEE, 2014, pp. 1–4.
[8] W. Ahn, S. Jung, W. Lee, S. Kim, J. Park, J. Shin, H. Kim, and K. Koo, "Design of coupled resonators for wireless power transfer to mobile devices using magnetic field shaping," in *Electromagnetic Compatibility (EMC), 2012 IEEE International Symposium on*. IEEE, 2012, pp. 772–776.
[9] Y. Lim and J. Park, "A novel phase-control-based energy beamforming techniques in nonradiative wireless power transfer," *IEEE Transactions on Power Electronics*, vol. 30, no. 11, pp. 6274–6287, 2015.
[10] Q. Zhu, M. Su, Y. Sun, W. Tang, and A. P. Hu, "Field orientation based on current amplitude and phase angle control for wireless power transfer," *IEEE Transactions on Industrial Electronics*, vol. 65, no. 6, pp. 4758–4770, 2018.
[11] M. Liu, M. Fu, and C. Ma, "Parameter design for a 6.78-mhz wireless power transfer system based on analytical derivation of class e current-driven rectifier," *IEEE Transactions on Power Electronics*, vol. 31, no. 6, pp. 4280–4291, 2016.